Title: Ptbp1 deletion does not induce glia-to-neuron conversion in adult mouse retina and brain.

Authors: Thanh Hoang[1*†], Dong Won Kim[1*†], Haley Appel[1], Nicole A. Pannullo[1], Manabu Ozawa[7], Sika Zheng[8], Minzhong Yu[9,10], Neil S. Peachey[9,10], Juhyun Kim[2], and Seth Blackshaw[1,3-6†].

Affiliations: [1]Solomon H. Snyder Department of Neuroscience, [2]Department of Psychiatry and Behavioral Science, [3]Department of Ophthalmology, [4]Department of Neurology, [5]Institute for Cell Engineering, [6]Kavli Neuroscience Discovery Institute, Johns Hopkins University School of Medicine, Baltimore, MD, USA; [7]Center for Experimental Medicine and Systems Biology, University of Tokyo, Tokyo, Japan; [8]Division of Biomedical Sciences, University of California, Riverside, CA; [9]Department of Ophthalmic Research, Cole Eye Institute; [10]Department of Ophthalmology, Cleveland Clinic Lerner College of Medicine of Case Western Reserve University, Cleveland, OH, USA.
  *Indicates equal contribution. †To whom correspondence should be addressed at vhoang3@jhmi.edu (TH), dkim195@jhmi.edu (DWK), and sblack@jhmi.edu (SB).

Abstract:

Somatic reprogramming of glia into neurons is a potentially promising approach for the replacement of neurons lost to injury or neurodegenerative disorders. Knockdown of the polypyrimidine tract-binding protein *Ptbp1* has been recently reported to induce efficient conversion of retinal Müller glia and brain astrocytes into functional neurons. However, genetic analysis of *Ptbp1* function in adult glia has not been conducted. Here, we use a combination of genetic lineage tracing, scRNA-Seq, and electrophysiological analysis to show that specific deletion of *Ptbp1* in adult retinal Müller glia and brain astrocytes does not lead to any detectable level of glia-to-neuron conversion. Few changes in gene expression are observed in glia following *Ptbp1* deletion, but glial identity is maintained. These findings highlight the importance of using genetic manipulation and lineage tracing methods in studying cell type conversion.

Introduction:

Neurodegenerative disorders are clinically diverse and represent a huge public health burden. To address this, considerable effort has been focused on directed transdifferentiation of endogenous glial cells into functional neurons that were lost to diseases. Most strategies to achieve this have included glial-specific viral overexpression of genes that promote neuronal identity, including transcription factors and miRNAs (Jorstad et al. 2017; Berninger et al. 2007; Cervo et al. 2017; Y. Liu et al. 2015; Caiazzo et al. 2011), or genetic or small molecule-based manipulation of extracellular signaling pathways (Zhang et al. 2015; Zamboni et al. 2020). These approaches have met with variable rates of success, with many treatments working only *in vitro* or in immature glia, inducing only partial reprogramming, or not generating desired neuronal subtypes (Vignoles et al. 2019). Furthermore, studies that reported highly efficient reprogramming using these approaches have been criticised for lacking data that unambiguously demonstrate a lineage relationship between reprogrammed glia and neurons (Blackshaw and Sanes 2021; C. Qian et al. 2021).

The ability to reliably and efficiently induce glial reprogramming *in vivo* by manipulation of a single factor would be a major advance towards effective cell-based therapy for

1

neurodegenerative disorders. Several recent reports have claimed to achieve exactly this outcome through knockdown of *Ptbp1* expression in retinal Müller glia and brain astrocytes (Zhou et al. 2020; H. Qian et al. 2020; Maimon et al. 2021; Fu et al. 2020). *Ptbp1* is an RNA binding protein and splicing regulator that is broadly expressed in non-neuronal and neuronal progenitor cells, and which represses neuronal-specific alternative splicing (Boutz et al. 2007; Makeyev et al. 2007).   Neural progenitor-specific deletion of *Ptbp1* leads to precocious neurogenesis (Shibasaki et al. 2013), and knockdown of *Ptbp1* has been reported to be sufficient to convert both fibroblast and N2a cells into neurons *in vitro* (Xue et al. 2013). Furthermore, several recent papers reported that knockdown of *Ptbp1* is sufficient to induce glial conversion into neurons. One study reported that *Ptbp1* knockdown in retinal Müller glia using AAV-mediated CasRx led to rapid and efficient transdifferentiation of Müller glia into retinal ganglion cells, which were then able to efficiently innervate targets in the brain following excitotoxic inner retinal injury (Zhou et al. 2020). This same study also reported that *Ptbp1* knockdown was sufficient for efficient conversion of brain astrocytes into dopaminergic neurons in the striatum and rescued function in a 6-OHDA-induced mouse model of Parkinson's disease (PD). A second study showed that lentiviral-mediated shRNA and antisense oligonucleotides (ASO)-mediated knockdown of *Ptbp1* in astrocytes in the cortex, striatum, and substantia nigra all induced efficient reprogramming of astrocytes into functional neurons, which in turn also rescued neurological defects in this same PD model (H. Qian et al. 2020). Other studies have reported that *Ptbp1* knockdown can convert retinal Müller glia to photoreceptors (Fu et al. 2020), and restore neurogenic competence in neural progenitor cells in the dentate gyrus of aged mice (Maimon et al. 2021).

        This simple and elegant loss of function approach potentially addresses many of the difficulties associated with previous efforts towards directed glial reprogramming, particularly in a clinical setting, such as low reprogramming efficiencies and the use of complex overexpression constructs. However, several major concerns remain to be addressed. First, none of these approaches convincingly demonstrated a reduction of *Ptbp1* expression in glial cells *in situ*. Second, lineage relationships between glia and neurons were inferred through the use of GFAP promoter-based AAV constructs or transgene, which are known to show neuronal expression in some contexts (Su et al. 2004; Fujita et al. 2014). Third, convincing evidence for direct glia-to-neuron conversion using reliable genetic lineage analysis and/or scRNA-Seq-based trajectory analysis is lacking. These concerns need to be addressed before the *Ptbp1* knockdown approach can further advance toward clinical applications.

        In this study, we address the question of knockdown specificity and efficiency of glia-to-neuron conversion upon *Ptbp1* reduction, through the use of glial-specific conditional mutants of *Ptbp1*, combining both genetic lineage and scRNA-Seq analysis of adult wildtype Müller glia and astrocytes, as well as adult glia carrying heterozygous or homozygous mutants of *Ptbp1*. Although we observe efficient and cell-specific disruption of *Ptbp1*, we observe no evidence for conversion of Müller glia or astrocytes into neurons in either heterozygous or homozygous *Ptbp1* mutants. ScRNA-Seq analysis reveals only subtle changes in gene expression in mutant glia, but no evidence for induction of neuronal-specific genes and no presence of neuronal physiology in mutant glia. Our data indicate that the glia-to-neuron conversion reported in previous studies following *Ptbp1* knockdown does not reflect the effects of *Ptbp1* loss of function.

Results:

Genetic loss of function of *Ptbp1* in retinal Müller glia did not lead to glia-to-neuron conversion.

To simultaneously disrupt *Ptbp1* in adult retinal Müller glia and irreversibly label these cells with a visible marker, we used three transgenic lines: *Glast^{CreERT2}*, which efficiently and selectively induces Cre-dependent recombination in Müller glia following tamoxifen treatment (de Melo et al. 2012; Hoang et al. 2020); *Sun1-GFP$^{lox/lox}$*, which expresses GFP targeted to the nuclear envelope under the ubiquitous CAG promoter following Cre activation (Mo et al. 2015); and *Ptbp1$^{lox/lox}$*, in which *loxP* sites flank the promoter and the first coding exon of *Ptbp1,* and Cre activation disrupts transcription (Shibasaki et al. 2013). We then generated wildtype (*Glast^{CreERT2}*;*Sun1-GFP$^{lox/lox}$*; *Ptbp1$^{+/+}$*), heterozygous (*Glast^{CreERT2}*;*Sun1-GFP$^{lox/lox}$*; *Ptbp1$^{lox/+}$*), and homozygous (*Glast^{CreERT2}*;*Sun1-GFP$^{lox/lox}$*; *Ptbp1$^{lox/lox}$*) mutant mice. Starting at ~5 weeks old, we induced Cre activation by using 4 doses of daily injections of 4-Hydroxytamoxifen (4-OHT) and conducted immunohistochemical analysis 2 and 4 weeks later (Fig. 1A).

Immunohistochemistry data shows that PTBP1 protein expression is enriched in Müller glia and some other non-glial cells in adult wildtype retinas (Fig. 1B). We observe that Cre activation led to a ~ 90% reduction in the number of PTBP1-positive Müller glia cells at both 2 and 4 weeks following 4-OHT induction in the homozygous retinas (Fig. 1B, C). GFP-positive nuclei of Müller glia remain confined to the inner nuclear layer, implying that they do not generate either retinal ganglion cells or photoreceptors (Fig. 1B). To confirm this finding, we then conducted immunostaining for the ganglion cell-specific markers RBPMS (Fig.1D, Fig. S1C) and BRN3B (Fig. S1D-E). In contrast to a recent report (Zhou et al. 2020), we did not observe any colocalization of these markers with GFP following *Ptbp1* deletion. We likewise observed no colocalization of the cone-specific marker arrestin (Fig. 1E) or the photoreceptor and bipolar marker OTX2 (Fig. S1F) with GFP, in contrast to another recent study (Fu et al. 2020). No induction of GFAP expression was observed in *Ptbp1*-deficient Müller glia (Fig. S1G), indicating that *Ptbp1* depletion did not initiate reactive gliosis. It had also been previously reported the robust conversion of Müller glia to retinal ganglion cells induced by *Ptbp1* depletion resulted in restoration of visual function following excitotoxic NMDA damage (Zhou et al. 2020). Although NMDA treatment led to extensive loss of RBPMS-positive retinal ganglion cells, we likewise did not observe any GFP/RBPMS or GFP/BRN3B-positive cells nor the recovery of retinal ganglion cells after 4 weeks following NMDA injury (Fig. 1F-G, S1H). Together, our data demonstrate that loss of *Ptbp1* does not convert Müller glia into retinal neurons either in healthy or damaged retinas.

Genetic loss of function of *Ptbp1* in brain astrocytes did not lead to glia-to-neuron conversion in the brain.

To genetically disrupt *Ptbp1* function in astrocytes, we employed a similar approach as in the retina, using astrocyte-specific tamoxifen-inducible *Aldh1l1^{CreERT2}* mice (Srinivasan et al. 2016), as well as the S*un1-GFP$^{lox/lox}$* and *Ptbp1$^{lox/lox}$* lines. We used the same breeding and tamoxifen induction strategy as in the retina to generate mice that were wildtype, heterozygous and homozygous for *Ptbp1* loss of function in astrocytes, and at the same time we irreversibly labeled astrocytes with Sun1-GFP for lineage tracing. Immunohistochemical analysis was then performed at 2 and 8 weeks following 4-OHT i.p induction (Fig. 2A).

As previous studies have reported glia-to-neuron conversion following *Ptbp1* knockdown in cortex, striatum, and substantia nigra (Zhou et al. 2020; H. Qian et al. 2020), we focused our analysis on these 3 brain regions. We observed a dramatic reduction in the percentage of PTBP1/GFP-double positive cells relative to total GFP-positive cells in homozygous mice in all three regions compared to wildtype, and a modest reduction in the heterozygotes relative to wildtype mice in cortex and striatum (Fig. 2B-C, Fig. S2). However, we did not observe any GFP-positive cells co-labeled with the neuronal markers NeuN and HuC/D in these regions in any genotypes, at either 2 or 8 weeks following 4-OHT i.p induction (Fig. 2D-F, Fig. S3A-C). Since previous studies had reported that *Ptbp1* knockdown induced markers of dopaminergic neurons in striatum and substantia nigra (Zhou et al. 2020; H. Qian et al. 2020), we then tested whether *Ptbp1* deletion induced either tyrosine hydroxylase (TH) or the dopaminergic transporter (DAT). However, we did not observe any colocalization of GFP with either marker in either region, regardless of the genotype (Fig. 2G-H, Fig. S3D-E).

We next examined if there is any potential effect of *Ptbp1* deletion on astrocyte physiology. No GFP-positive astrocytes in the cortex, in either *Ptbp1* heterozygotes and homozygotes, fired action potentials in response to the current steps in whole-cell patch-clamp recordings, whereas neighboring GFP-negative wildtype neurons readily fired action potentials (Fig. 3A). This indicates that *Ptbp1* deletion did not change the electrophysiological functions of astrocytes to make them fire action potentials like neurons. The astrocytes displayed highly negative resting membrane potentials (Ptbp1-Het, -82.2 ± 1.1 mV; Ptbp1-KO, -81.4 ± 1.9 mV) as previously reported (McNeill et al. 2021), and the *Ptbp1* heterozygous and homozygous cells did not show significant difference in resting membrane potential (Fig. 3B, p=0.7795, Mann-Whitney test). These results suggest that *Ptbp1* deletion in astrocytes does not induce any specific neuronal-like electrophysiological changes.

Genetic loss of function of *Ptbp1* leads to only subtle changes in the gene expression profile of Müller glia and astrocytes

Previous studies did not characterize the gene expression profile of glial cells after *Ptbp1* knockdown (Zhou et al. 2020; H. Qian et al. 2020). To comprehensively profile the cellular phenotype induced by *Ptbp1* deletion in Müller glia and astrocytes, we performed scRNA-Seq analysis of retina, cortex, striatum, and substantia nigra 2 weeks following tamoxifen treatment of wildtype, heterozygous, and homozygous mice (Fig. 3C, G). Müller glia and astrocytes were then subsetted for further analysis (Fig. 3D, 3I, S4A, B, S5A).

In all tissues, we see a consistent reduction in *Ptbp1* expression levels in Müller glia or astrocytes in heterozygous and homozygous mice (Fig. 3E, Fig.S5E). The relative fraction of either Müller glia or any major subtype of retinal neurons did not obviously change among any of the genotypes (Fig. S4B). We observe few significant changes in gene expression in any glial population profiled. In Müller glia, we observe increased expression of the *Ptbp1* paralogue *Ptbp2* expression level following *Ptbp1* disruption (Fig. 3F). *Ptbp2* upregulation has previously been reported in neural progenitors following *Ptbp1* loss of function (Boutz et al. 2007), and since *Ptbp1* and *Ptbp2* show partially redundant functions (Vuong et al. 2016), this may provide some functional compensation for *Ptbp1* loss of function. We also observe increased expression of *Id3, Trf, Eno1, Mt3, Lgals3,* with reduced expression of *Msi2, Dio2, Rnf121, Atp1a2* (Fig. 3F). In all cases, the changes in gene expression were quite modest (Table ST1);

4

we did not observe either significant reductions of expression of Müller glia-specific markers, including *Sox9*, *Glul*, *Rlbp1*, *Slc1a3*, *Apoe*, *Aqp4*, *Mlc1*, *Kcnj10,* and *Tcf7l2*, or induction of genes specific to neural progenitors or mature neurons (Fig. S4D, Table ST1). Immunostaining confirmed that *Ptbp1*-deficient Müller glia retained expression of the glial marker SOX9 (Fig. S4E). Together, our data demonstrate that loss of function of *Ptbp1* does not dramatically alter gene expression in Müller glia, or cause these cells to lose their identity.

We likewise did not observe any clear changes in the astrocytes across the 3 genotypes in any of the brain regions (Fig. 3H-I, Table ST2-ST4). A correlation plot showed that differences in gene expression in astrocytes among brain regions (cortex and striatum to substantia nigra) were higher than the differences among genotypes (Fig. 3H). We also observed *S100b*-expressing astrocytes in the striatum as previously reported (Gokce et al. 2016) (Fig. S5D). As with Müller glia, we observed only very modest changes in gene expression following *Ptbp1* loss of function (Fig. 3J, Table ST2-ST4). Upregulated genes include *mt-Nd4, Son, Hes5, Mt3*; downregulated genes include *mt-Nd3, Lars2, Ivd*. Most astrocyte markers did not show altered expression after *Ptbp1* deletion (Fig. S5F). Immunostaining confirmed that *Ptbp1*-deficient, GFP-positive astrocytes retained expression of glial marker SOX9 (Fig. S5G). We also do not observe induction of either neural progenitor or mature neuron-specific genes (Table ST2-ST4). We conclude that *Ptbp1* does not function in mature glial cells to repress the expression of neuronal genes.

Discussion:

Using the genetic loss of function and cell lineage analysis, in combination with scRNA-Seq analysis, we observed no evidence that either partial or complete loss of function of *Ptbp1* induces glia-to-neuron conversion in retina or brain. Our data contrasts sharply with several recent studies that analyze the effects of *Ptbp1* knockdown using ASO, shRNA, and/or CasRx (Zhou et al. 2020; H. Qian et al. 2020; Fu et al. 2020; Maimon et al. 2021), but is in agreement with a recent study the re-examined previous studies reporting astrocyte-to-neuron conversion following *Neurod1* overexpression or either shRNA- or CasRx-mediated *Ptbp1* knockdown (Wang et al. 2021). This latter study concluded that reports of glia-to-neuron conversion in these two models represented a leaky neuronal expression of the GFAP-based AAV and transgene lines used to label astrocytes. Leaky neuronal expression of GFAP-based reagents has been previously reported in other contexts (Su et al. 2004; Fujita et al. 2014), and caution should be used when interpreting results obtained using these methods without corroborating data obtained using more strongly glial-specific minipromoters and Cre lines, such as the extensively validated *Glast^CreERT2* and *Aldh1l1^CreERT2* lines used here.

Our data show that the previous reports of glia-to-neuron conversion is unlikely to have resulted from *Ptbp1* loss of function in glial cells. Then what could have accounted for the recovery of visual function following NMDA excitotoxicity, or behavioral recovery following 6-OHDA-induced PD (Zhou et al. 2020; H. Qian et al. 2020)? Ectopic neuronal expression of GFAP-based reagents in endogenous native neurons represents one possible explanation. For example, inclusion of the Ptbp1-dependent control of splicing of proapoptotic gene *Bak1* is essential for neuronal and animal survival (Lin et al. 2020). Knockdown of residual PTBP1 expression in neurons may therefore further promote neuronal survival. Another possibility is unexpected beneficial off-target effects of reagents targeting *Ptbp1* in the previous reports. In

either case, genetic methods should be used to validate future reports of glia-to-neuron conversion.

Figure legends:

Figure 1. *Ptbp1* deletion does not result in the conversion of Müller glia into retinal neurons in adult mice. (**A**) A schematic diagram of the generation of specific *Ptbp1* deletion and lineage tracing of Müller glia. (**B**) Representative immunohistochemistry of PTBP1 expression in wildtype (Ptbp1-Ctrl), heterozygous (Ptbp1-Het) and homozygous (Ptbp1-KO) *Ptbp1* retinas after 4 weeks of 4-OHT i.p injection. White arrowheads indicate residual Ptbp1-expressing Müller glial cells. (**C**) Quantification of the percentage of PTBP1/GFP-double positive Müller glial cells after 2 and 4 weeks of 4-OHT i.p injection (n >= 4 retinas/genotype). (**D**) Representative immunohistochemistry for RBPMS, a pan-retinal ganglion cell marker, in retinal sections from three genotypes (n >= 6 retinas/genotype) after 4 weeks of 4-OHT i.p injection. (**E**) Representative images of immunohistochemical analysis of cone Arrestin in retinal sections from three genotypes after 4 weeks of 4-OHT i.p injection (n >= 3 retinas/genotype). (**F**) Representative immunohistostaining of RBPMS in retinal sections from the three genotype groups at 6 weeks after NMDA injury (n >= 3 retinas/genotype). White arrowheads indicate residual RBPMS-expressing ganglion cells. (**G**) Quantification of RBPMS-positive cells in wildtype, heterozygous and homozygous *Ptbp1* mutant retinas (n >= 4 retinas/genotype) with or without NMDA injury. ONL, outer nuclear layer; INL, inner nuclear layer; GCL, ganglion cell layer. Scale bars = 100 μm.

Figure 2. Loss of Ptbp1 did not result in astrocyte-to-neuron conversion in the adult mouse brain. (**A**) A schematic diagram for the generation of specific deletion of *Ptbp1* and lineage tracing of astrocytes, and experimental timelines. (**B**) Representative PTBP1 and GFP immunostaining images of the cortex at 8 weeks after 4-OHT i.p injection. Yellow arrows indicate PTBP1/GFP-double positive cells (n=3 mice/genotype). White arrowheads indicate PTBP1-negative/GFP-positive cells. (**C**) Quantification of the percentage of PTBP1/GFP-double positive cells showing a highly efficient *Ptbp1* deletion in all three brain regions (cortex, striatum, and substantia nigra). (**D-F**) Representative immunostaining images of HuC/D;NeuN and GFP in the cortex (D), striatum (E), and substantia nigra (F) at 8 weeks after 4-OHT i.p injection. No HuCD;NeuN/GFP+double positive cells were observed in any of the three brain regions (n=3 mice/genotype). (**G-H**) Representative immunostaining images of TH and GFP in the striatum (G), and substantia nigra (J) at 8 weeks after 4-OHT i.p injection. No TH/GFP+double positive cells were observed in any of the two brain regions (n=3 mice/genotype). Scale bars = 50 μm.

Figure 3. No changes in electrophysiological properties of cortical astrocytes, and only subtle changes in gene expression in Müller glia and astrocytes, are observed after *Ptbp1* deletion. (**A**) Representative cell images and voltage traces to the depolarizing current steps of a GFP-positive cell from Ptbp1-Het (left), Ptbp1-KO mice (middle), and a GFP-negative neuron from a Ptbp1-KO mouse (right). Yellow arrows indicate the location of the recorded cells in bright and fluorescence images. Scale bar = 40 μm. (**B**) A summary graph for resting membrane potential (RMP) of the GFP-positive cells between groups (Ptbp1-Het, 12 cells from

6

3 mice; Ptbp1-KO, 14 cells from 3 mice). (**C**) A schematic diagram of scRNA-Seq experiments in *Glast*^{CreERT2};*Sun1-GFP*$^{lox/lox}$; *Ptbp1*$^{+/+}$, *Glast*^{CreERT2};*Sun1-GFP*$^{lox/lox}$; *Ptbp1*$^{lox/+}$, *Glast*^{CreERT2};*Sun1-GFP*$^{lox/lox}$; *Ptbp1*$^{lox/lox}$ retina. (**D**) UMAP plot showing subsetted retinal Müller glia from all 3 genotypes. Note that there are no separated *Ptbp1* knockout Müller glia clusters. (**E**) Violin plot showing *Ptbp1* RNA expression in Müller glia across the 3 genotypes. (**F**) Dot plot showing some mildly changing genes of Müller glia across the 3 genotypes. (**G**) A schematic diagram of scRNA-Seq experiments in *Aldh1l1*^{CreERT2};*Sun1-GFP*$^{lox/lox}$; *Ptbp1*$^{+/+}$, *Aldh1l1*^{CreERT2};*Sun1-GFP*$^{lox/lox}$; *Ptbp1*$^{lox/+}$, *Aldh1l1*^{CreERT2};*Sun1-GFP*$^{lox/lox}$; *Ptbp1*$^{lox/lox}$ in the brain. (**H**) Heatmap showing a correlation in subsetted astrocytes across genotypes and brain regions. (**I**) UMAP plot showing subsetted astrocytes in the cortex (left), striatum (middle), and substantia nigra (right) of all 3 genotypes. Note that there are no separated *Ptbp1* knockout astrocyte clusters. (**J**) Dot plot showing some mildly changing genes in subsetted astrocytes in the cortex (left), striatum (middle), and substantia nigra (right) across genotypes. Ctx = Cortex, Str = Striatum, SN = Substantia nigra.

Supplemental figure legends:

Figure S1. Immunohistochemical characterization of adult mouse retinas with Müller glia-specific *Ptbp1* deletion. (**A**, **B**) A schematic diagram of the generation of specific *Ptbp1* deletion and lineage tracing of Müller glia and experimental timelines. (**C, D**) Representative immunostaining for RBPMS and BRN3B expression in adult wildtype, heterozygous and homozygous *Ptbp1*-deleted mouse retinas after 2 weeks of 4-OHT i.p injection. No RBPMS/GFP+double positive or BRN3B/GFP+double positive were observed in any of the three brain regions (n=3 mice/genotype). (**E**, **F, G**) Representative images of immunohistochemical analysis for BRN3B, OTX2, and GFAP expression in the retinas of the three genotypes after 4 weeks of 4-OHT i.p injection. No BRN3B/GFP+double positive or OTX2/GFP+double positive were observed in any of the three brain regions (n=3 mice/genotype). (**H**) Efficient depletion of BRN3B-positive retinal ganglion cells in all three genotypes after 6 weeks of intravitreal NMDA injection. White arrowheads indicate remaining BRN3B-positive retinal ganglion cells that survived. ONL, outer nuclear layer; INL, inner nuclear layer; GCL, ganglion cell layer. Scale bars = 100 μm.

Figure S2. *Ptbp1* immunohistochemical analysis in adult mouse brain after astrocyte-specific deletion of *Ptbp1*. (**A-C**) Representative PTBP1 and GFP immunostaining images of the cortex (A), striatum (B), substantia nigra (C) at 8 weeks after 4-OHT i.p injection. Note that the same cortical images in Fig. 2A were used in panel A, but are shown here using higher magnification. Scale bars = 50 μm.

Figure S3. Immunohistochemical analysis of adult mouse brain after astrocyte-specific deletion of *Ptbp1*. (**A-C**) Representative HuC/D;NeuN and GFP immunostaining images of the cortex (A), striatum (B), substantia nigra (C) at 2 weeks after 4-OHT i.p injection (n=3 mice/genotype). No HuCD;NeuN/GFP-double positive cells were observed in any of the three brain regions. (**D, E**) Representative DAT and GFP immunostaining images of the striatum (D), substantia nigra (E) at 8 weeks after 4-OHT i.p injection. No DAT/GFP+double positive cells were observed in any of the two brain regions. Scale bars = 50 μm.

Figure S4. ScRNA-analysis of mouse retinas after Müller glia-specific *Ptbp1* deletion. (**A, B**) UMAP plots showing scRNA-Seq clusters of all 3 combined genotypes (A) and separately (B), and the percentage of Müller glia in each scRNA-Seq dataset. (**C**) Gene plots of representative Müller glia markers, *Sox9* and *Slc1a3*. (**D**) Violin plot showing no significant change in the expression of Müller glia markers across 3 genotypes. (**E)** Representative SOX9 and GFP immunostaining images of the retina from 3 genotypes at 4 weeks after 4-OHT i.p injection (n=4 mice/genotype). ONL, outer nuclear layer; INL, inner nuclear layer; GCL, ganglion cell layer. Scale bars = 100 μm.

Figure S5. ScRNA-analysis of mouse brain after astrocyte-specific *Ptbp1* deletion. (**A-C**) UMAP plots showing scRNA-Seq clusters of all 3 genotypes (top) and gene plots of representative neuronal markers and astrocyte markers in the cortex (A), striatum (B), and substantia nigra (C), and the percentage of astrocytes in each scRNA-Seq dataset across 3 genotypes. (**D**) Gene plot showing 2 sub-clusters in striatum astrocytes. (**E**) Dot plot showing *Ptbp1* expression in subsetted astrocytes in the 3 brain regions across 3 genotypes. (**F**) Violin plot showing expression of astrocyte-enriched genes in subsetted astrocytes across 3 genotypes. (**G)** Representative SOX9 and GFP immunostaining images of the cortex, striatum, and substantia nigra after at 8 weeks 4-OHT i.p injection. Orange arrows indicate SOX9-positive astrocytes, and white arrowheads indicate SOX9-negative astrocytes. Scale bars = 50 μm.

Supplemental Tables:
Supplemental Table 1 - Differential gene expression as measured by scRNA-Seq in retinal Müller glia across *Ptbp1* genotypes.
Supplemental Table 2 - Differential gene expression as measured by scRNA-Seq in cortical astrocytes across *Ptbp1* genotypes.
Supplemental Table 3 - Differential gene expression as measured by scRNA-Seq in striatal astrocytes across *Ptbp1* genotypes.
Supplemental Table 4 - Differential gene expression as measured by scRNA-Seq in substantia nigra astrocytes across *Ptbp1* genotypes.

Materials and Methods:
Mice

$Glast^{CreERT2}$ and $Sun1\text{-}GFP^{lox/lox}$ transgenic mice were provided by Dr. Jeremy Nathans (de Melo et al. 2012; Mo et al. 2015). $Aldh1l1^{CreERT2}$ transgenic mouse line, which allows for specific inducible Cre-recombination in astrocytes after TAM injection (Srinivasan et al. 2016), was purchased from JAX (JAX#029655). $Ptbp1^{lox/lox}$ mice carrying loxP sites that flank the promoter and 1st exon of $Ptbp1$ were generated as described previously (Shibayama et al. 2009). To induce specific Cre activation in adult Müller and astrocytes, 4 consecutive doses of 4-Hydroxytamoxifen (4-OHT) intraperitoneal (i.p) injection (30 mg/kg) were performed in adult wildtype, heterozygous and homozygous mice at ~5 weeks old. Mice were sacrificed at the indicated time for analysis.

Intravitreal NMDA injection

We followed a previously described protocol (Zhou et al. 2020). Briefly, adult mice were anesthetized with 4% isoflurane inhalation. 1.5 µl of 200 mM NMDA in PBS was injected intravenously into the retinas. 4 consecutive doses of 4-OHT i.p injection (30 mg/kg) were performed at 2 weeks after NMDA injection. Mice were sacrificed, and retinas were collected at 4 weeks after 4-OHT injection.

Immunohistochemical and imaging analysis

Retinal collection and immunohistochemical analysis were performed as described previously (Hoang et al. 2020). Briefly, mice were anesthetized by CO_2, and eye globes were fixed in 4% paraformaldehyde in PBS for 4 hr at room temperature. Retinas were dissected and placed into 30% sucrose in PBS at 4°C overnight. Retinas were embedded in OCT, sectioned at 16 µm thickness, and stored at -20C. Retinal sections were air-dried at 37°C for 20 min, washed 3 x 5 mins with PBS times, and incubated in a blocking buffer (0.4% TritonX-100, 10% horse serum in PBS) for 1 hr at room temperature. Primary antibodies were incubated in the blocking buffer at the indicated concentration overnight at 4°C. Primary antibodies used in this study were: rabbit anti-Ptbp1(1:200, Proteintech, #125821-AP), rabbit Rbpms (1:200, Proteintech, #151871-AP), goat anti-Brn3b (1:200, Santa Cruz, #sc6026), rabbit anti-cone arrestin (1:200, Millipore Sigma, #AB15282), goat anti-Otx2 (1:200, R&D systems, #AF1979), rabbit anti-Gfap (1;300, Dako, #z0334), rabbit anti-Sox9 (1:200, Millipore Sigma, #AB5535), rabbit anti-GFP (1:400, Life technologies, #A6455) and chicken anti-GFP (1:400, Thermo Fisher Scientific, #A10262). Secondary antibodies were incubated at 1:400 dilution in the blocking buffer. Retinal sections were then incubated with DAPI, washed 4 x 5 min in PBS, mounted with prolong gold mounting media (ThermoFisher Scientific, #P36935), air-dried, and stored in 4°C.

Brain collection and immunohistochemical analysis were performed as described previously (Hoang et al. 2020; Kim et al. 2020; Yoo et al. 2019). Briefly, mice were anesthetized by avertin and cardially perfused with 4% paraformaldehyde. Brains were then dissected and post-fixed in 4% paraformaldehyde for 12 hr at room temperature, and then placed into 30% sucrose in PBS at 4°C overnight. Brains were sectioned at 30 µm thickness and processed for immunohistochemistry as described above. Additional primary antibodies used in this study for the brain were: mouse anti-HuC/D (1:200, Thermo Fisher Scientific, #A21271), mouse anti-NeuN (1:200, Millipore Sigma, #MAB377), rat anti-Dopamine Transporter Antibody (DAT, 1:200,

Millipore Sigma, #MAB369), rabbit anti-Tyrosine Hydroxylase (TH, 1:200, Millipore Sigma, #AB152).

Images were acquired using Zeiss LSM700 confocal microscope at > 6 random regions for each retina or brain. Images were processed using ImageJ.

Electroretinogram

Slice electrophysiology of cortical astrocytes
The acute brain slices were generated as previously described (K. Liu et al. 2017; Yoo et al. 2021). Ptbp1-Het or Ptbp1-KO (P54 to P73, male) were anesthetized with isoflurane and decapitated, and the brains were rapidly removed and chilled in ice-cold sucrose solution containing 76 mM NaCl, 25 mM NaHCO3, 25 mM glucose, 75 mM sucrose, 2.5 mM KCl, 1.25 mM NaH2PO4, 0.5 mM CaCl2, and 7 mM MgSO4 (pH 7.3). Acute brain slices (300 μm) including the motor cortex were prepared using a vibratome (VT 1200 s, Leica) and transferred to warm (32° to 35°C) sucrose solution for 30 min for recovery. The slices were transferred to warm (32° to 34°C) aCSF composed of 125 mM NaCl, 26 mM NaHCO3, 2.5 mM KCl, 1.25 mM NaH2PO4, 1 mM MgSO4, 20 mM glucose, 2 mM CaCl2, 0.4 mM ascorbic acid, 2 mM pyruvic acid, and 4 mM l-(+)-lactic acid (pH 7.3, 315 mOsm) and allowed to cool to room temperature. All solutions were continuously bubbled with 95% O2/5% CO2.

For whole-cell patch-clamp recordings, slices were transferred to a submersion chamber on an upright microscope [Zeiss Axio Examiner, objective lens: 5×, 0.16 numerical aperture (NA) and 40×, 1.0 NA] fitted for infrared differential interference contrast (IR-DIC) and fluorescence microscopy. Slices were continuously superfused (2 to 4 ml/min) with warm, oxygenated aCSF (32° to 34°C). Sun1-GFP(+) cells in the layer 2/3 of the motor cortex were identified under a digital camera (Sensicam QE, Cooke) using transmitted light and green fluorescence. For the whole-cell patch-clamp recordings, borosilicate glass pipettes (2 to 4 MΩ) were filled with an internal solution containing 2.7 mM KCl, 120 mM KMeSO4, 9 mM Hepes, 0.18 mM EGTA, 4 mM Mg-adenosine 5′-triphosphate, 0.3 mM Na-guanosine 5′-triphosphate, and 20 mM phosphocreatine(Na) (pH 7.3, 295 mOsm). Whole-cell patch-clamp recordings were conducted through a MultiClamp 700B amplifier (Molecular Devices) and an ITC-18 (InstruTECH), which were controlled by customized routines written in Igor Pro (WaveMetrics).

To determine the action potential firing capacity of the recorded cells, a series of depolarizing current steps (1-s long, 0 to 4000 pA) was given to the cells, and their voltage responses were recorded. During the current step test, cells were held at their resting membrane potentials, and different intensities of currents were tested until the cell membrane potential went over 0 mV without firing action potentials or the membrane potential did not hold from 4000 pA current injections. As a control, three Sun1-GFP(-) neurons from two Ptbp1-KO mice were targeted and their voltage responses to a series of depolarizing current steps (1-s long, 0 to 300 pA) were recorded by using the same internal and external solutions for comparing action potential firing properties with Sun1-GFP(+) cells from the same mice. All signals were low-pass filtered at 10 kHz and sampled at 20 kHz. Electrophysiology data was analyzed in Igor Pro (WaveMetrics).

Cell dissociation and scRNA-Seq

Retinal cell dissociation was performed as described previously (Hoang et al. 2020). Briefly, one female mouse per genotype was euthanized by CO_2, and eye globes were removed and placed in ice-cold PBS. Retinas were dissected, cells were dissociated using Papain Dissociation System (LK003150, Worthington). Dissociated cells were resuspended in a buffer containing 9.8ml Hibernate A, 200µl B27, 20 µl GlutaMAX and 0.5U/ul RNAse inhibitor. Cells were filtered through a 50µm filter. Cell count and viability were determined by using 0.4% Trypan blue.

Brain cell dissociation was performed as described previously (Bell et al. 2021; Kim et al. 2021) using one female mouse per genotype. Mouse brain matrix (0.5 mm) was used to slice brains into coronal sections, and relative brain regions (cerebral cortex, striatum, midbrain) were dissected into Hibernate-A media with a 2% B-27 and GlutaMAX supplement (0.5 mM final). Tissues were dissociated in papain (Worthington).

Cells were then loaded into the 10x Genomics Chromium Single Cell System (10x Genomics) and libraries were generated using v3.1 chemistry following the manufacturer's instructions. Libraries were sequenced on the Illumina NovaSeq platform (500 million reads per library).

ScRNA-Seq data analysis
Sequencing data were first processed through the Cell Ranger (v.6.0.1, 10x Genomics) with default parameters, aligned to the mm10 genome (refdata-gex-mm10-2020-A), and matrix files were used for subsequent bioinformatic analysis.

Matrix data were further processed using Seurat 3.4 version (Stuart et al. 2019). Low quality cells with < 500 genes, < 2000 UMI and > 30% mitochondrial genes were removed. Datasets were normalized using Seurat 'scTransform' function. Cells were clustered and visualized using UMAP. Retinal Müller glia (*Slc1a3*+ & *Rlbp1*+) and brain astrocytes (*Slc1a3*+ & *Aldh1l1*+) clusters were subsetted for further analysis to compare differential gene expression across genotypes. Differential gene expression between different genotypes was calculated using the Seurat '*FindMarker'* function.

Author contributions: TH, DWK, and SB conceived and supervised the study. TH generated and analyzed immunohistochemistry and scRNA-Seq data from retina, assisted by HA, NAP, and TK. DWK generated and analyzed immunohistochemistry and scRNA-Seq data from brain, assisted by TH and HA. MO and SZ provided reagents. JK performed slice electrophysiology of cortical astrocytes. MY and NSP conducted ERG analysis. TH, DWK, and SB drafted the manuscript. All authors contributed to the writing of the manuscript.

Data availability: All scRNA-Seq data have been deposited to GEO as GSE184933.

References

Bell, Benjamin J., Annette A. Wang, Dong Won Kim, Jiali Xiong, Seth Blackshaw, and Mark N. Wu. 2021. "Characterization of mWake Expression in the Murine Brain." *The Journal of Comparative Neurology* 529 (8): 1954–87.

Berninger, Benedikt, Marcos R. Costa, Ursula Koch, Timm Schroeder, Bernd Sutor, Benedikt Grothe, and Magdalena Götz. 2007. "Functional Properties of Neurons Derived from in Vitro Reprogrammed Postnatal Astroglia." *The Journal of Neuroscience: The Official Journal of the Society for Neuroscience* 27 (32): 8654–64.

Blackshaw, Seth, and Joshua R. Sanes. 2021. "Turning Lead into Gold: Reprogramming Retinal Cells to Cure Blindness." *The Journal of Clinical Investigation* 131 (3). https://doi.org/10.1172/JCI146134.

Boutz, Paul L., Peter Stoilov, Qin Li, Chia-Ho Lin, Geetanjali Chawla, Kristin Ostrow, Lily Shiue, Manuel Ares Jr, and Douglas L. Black. 2007. "A Post-Transcriptional Regulatory Switch in Polypyrimidine Tract-Binding Proteins Reprograms Alternative Splicing in Developing Neurons." *Genes & Development* 21 (13): 1636–52.

Caiazzo, Massimiliano, Maria Teresa Dell'Anno, Elena Dvoretskova, Dejan Lazarevic, Stefano Taverna, Damiana Leo, Tatyana D. Sotnikova, et al. 2011. "Direct Generation of Functional Dopaminergic Neurons from Mouse and Human Fibroblasts." *Nature* 476 (7359): 224–27.

Cervo, Pia Rivetti di Val, Pia Rivetti di Val Cervo, Roman A. Romanov, Giada Spigolon, Débora Masini, Elisa Martín-Montañez, Enrique M. Toledo, et al. 2017. "Induction of Functional Dopamine Neurons from Human Astrocytes in Vitro and Mouse Astrocytes in a Parkinson's Disease Model." *Nature Biotechnology*. https://doi.org/10.1038/nbt.3835.

Fujita, Takumi, Michael J. Chen, Baoman Li, Nathan A. Smith, Weiguo Peng, Wei Sun, Michael J. Toner, et al. 2014. "Neuronal Transgene Expression in Dominant-Negative SNARE Mice." *The Journal of Neuroscience: The Official Journal of the Society for Neuroscience* 34 (50): 16594–604.

Fu, Xin, Jie Zhu, Yaou Duan, Gen Li, Huimin Cai, Lianghong Zheng, Hao Qian, et al. 2020. "Visual Function Restoration in Genetically Blind Mice via Endogenous Cellular Reprogramming." *bioRxiv*. https://doi.org/10.1101/2020.04.08.030981.

Gokce, Ozgun, Geoffrey M. Stanley, Barbara Treutlein, Norma F. Neff, J. Gray Camp, Robert C. Malenka, Patrick E. Rothwell, Marc V. Fuccillo, Thomas C. Südhof, and Stephen R. Quake. 2016. "Cellular Taxonomy of the Mouse Striatum as Revealed by Single-Cell RNA-Seq." *Cell Reports* 16 (4): 1126–37.

Hoang, Thanh, Jie Wang, Patrick Boyd, Fang Wang, Clayton Santiago, Lizhi Jiang, Sooyeon Yoo, et al. 2020. "Gene Regulatory Networks Controlling Vertebrate Retinal Regeneration." *Science* 370 (6519). https://doi.org/10.1126/science.abb8598.

Jorstad, Nikolas L., Matthew S. Wilken, William N. Grimes, Stefanie G. Wohl, Leah S. VandenBosch, Takeshi Yoshimatsu, Rachel O. Wong, Fred Rieke, and Thomas A. Reh. 2017. "Stimulation of Functional Neuronal Regeneration from Müller Glia in Adult Mice." *Nature* 548 (7665): 103–7.

Kim, Dong Won, Kai Liu, Zoe Qianyi Wang, Yi Stephanie Zhang, Abhijith Bathini, Matthew P. Brown, Sonia Hao Lin, et al. 2021. "Gene Regulatory Networks Controlling Differentiation, Survival, and Diversification of Hypothalamic Lhx6-Expressing GABAergic Neurons." *Communications Biology* 4 (1): 95.

Kim, Dong Won, Parris Whitney Washington, Zoe Qianyi Wang, Sonia Hao Lin, Changyu Sun, Basma Taleb Ismail, Hong Wang, Lizhi Jiang, and Seth Blackshaw. 2020. "The Cellular and Molecular Landscape of Hypothalamic Patterning and Differentiation from Embryonic to Late Postnatal Development." *Nature Communications* 11 (1): 4360.

Lin, Lin, Min Zhang, Peter Stoilov, Liang Chen, and Sika Zheng. 2020. "Developmental Attenuation of Neuronal Apoptosis by Neural-Specific Splicing of Bak1 Microexon." *Neuron*

107 (6): 1180–96.e8.

Liu, Kai, Juhyun Kim, Dong Won Kim, Yi Stephanie Zhang, Hechen Bao, Myrto Denaxa, Szu-Aun Lim, et al. 2017. "Lhx6-Positive GABA-Releasing Neurons of the Zona Incerta Promote Sleep." *Nature* 548 (7669): 582–87.

Liu, Yueguang, Qinglong Miao, Jiacheng Yuan, Su 'e Han, Panpan Zhang, Sanlan Li, Zhiping Rao, et al. 2015. "Ascl1 Converts Dorsal Midbrain Astrocytes into Functional Neurons In Vivo." *The Journal of Neuroscience: The Official Journal of the Society for Neuroscience* 35 (25): 9336–55.

Maimon, Roy, Carlos Chillon-Marinas, Cedric E. Snethlage, Sarthak M. Singhal, Melissa McAlonis-Downes, Karen Ling, Frank Rigo, et al. 2021. "Therapeutically Viable Generation of Neurons with Antisense Oligonucleotide Suppression of PTB." *Nature Neuroscience* 24 (8): 1089–99.

Makeyev, Eugene V., Jiangwen Zhang, Monica A. Carrasco, and Tom Maniatis. 2007. "The MicroRNA miR-124 Promotes Neuronal Differentiation by Triggering Brain-Specific Alternative Pre-mRNA Splicing." *Molecular Cell* 27 (3): 435–48.

McNeill, Jessica, Christopher Rudyk, Michael E. Hildebrand, and Natalina Salmaso. 2021. "Ion Channels and Electrophysiological Properties of Astrocytes: Implications for Emergent Stimulation Technologies." *Frontiers in Cellular Neuroscience* 15 (May): 644126.

Melo, Jimmy de, Katsuaki Miki, Amir Rattner, Phil Smallwood, Cristina Zibetti, Karla Hirokawa, Edwin S. Monuki, Peter A. Campochiaro, and Seth Blackshaw. 2012. "Injury-Independent Induction of Reactive Gliosis in Retina by Loss of Function of the LIM Homeodomain Transcription Factor Lhx2." *Proceedings of the National Academy of Sciences of the United States of America* 109 (12): 4657–62.

Mo, Alisa, Eran A. Mukamel, Fred P. Davis, Chongyuan Luo, Gilbert L. Henry, Serge Picard, Mark A. Urich, et al. 2015. "Epigenomic Signatures of Neuronal Diversity in the Mammalian Brain." *Neuron* 86 (6): 1369–84.

Qian, Cheng, Bryan Dong, Xu-Yang Wang, and Feng-Quan Zhou. 2021. "In Vivo Glial Trans-Differentiation for Neuronal Replacement and Functional Recovery in Central Nervous System." *The FEBS Journal* 288 (16): 4773–85.

Qian, Hao, Xinjiang Kang, Jing Hu, Dongyang Zhang, Zhengyu Liang, Fan Meng, Xuan Zhang, et al. 2020. "Reversing a Model of Parkinson's Disease with in Situ Converted Nigral Neurons." *Nature*. https://doi.org/10.1038/s41586-020-2388-4.

Shibasaki, Takayuki, Akinori Tokunaga, Reiko Sakamoto, Hiroshi Sagara, Shigeru Noguchi, Toshikuni Sasaoka, and Nobuaki Yoshida. 2013. "PTB Deficiency Causes the Loss of Adherens Junctions in the Dorsal Telencephalon and Leads to Lethal Hydrocephalus." *Cerebral Cortex* 23 (8): 1824–35.

Shibayama, Masaki, Satona Ohno, Takashi Osaka, Reiko Sakamoto, Akinori Tokunaga, Yuhki Nakatake, Mitsuharu Sato, and Nobuaki Yoshida. 2009. "Polypyrimidine Tract-Binding Protein Is Essential for Early Mouse Development and Embryonic Stem Cell Proliferation." *The FEBS Journal* 276 (22): 6658–68.

Srinivasan, Rahul, Tsai-Yi Lu, Hua Chai, Ji Xu, Ben S. Huang, Peyman Golshani, Giovanni Coppola, and Baljit S. Khakh. 2016. "New Transgenic Mouse Lines for Selectively Targeting Astrocytes and Studying Calcium Signals in Astrocyte Processes In Situ and In Vivo." *Neuron* 92 (6): 1181–95.

Stuart, Tim, Andrew Butler, Paul Hoffman, Christoph Hafemeister, Efthymia Papalexi, William M. Mauck, Yuhan Hao, Marlon Stoeckius, Peter Smibert, and Rahul Satija. 2019. "Comprehensive Integration of Single-Cell Data." *Cell*. https://doi.org/10.1016/j.cell.2019.05.031.

Su, Mu, Huimin Hu, Youngjin Lee, Alessandra d'Azzo, Albee Messing, and Michael Brenner. 2004. "Expression Specificity of GFAP Transgenes." *Neurochemical Research* 29 (11): 2075–93.

Vignoles, Rory, Célia Lentini, Marie d'Orange, and Christophe Heinrich. 2019. "Direct Lineage Reprogramming for Brain Repair: Breakthroughs and Challenges." *Trends in Molecular Medicine* 25 (10): 897–914.

Vuong, John K., Chia-Ho Lin, Min Zhang, Liang Chen, Douglas L. Black, and Sika Zheng. 2016. "PTBP1 and PTBP2 Serve Both Specific and Redundant Functions in Neuronal Pre-mRNA Splicing." *Cell Reports* 17 (10): 2766–75.

Wang, Lei-Lei, Carolina Serrano, Xiaoling Zhong, Shuaipeng Ma, Yuhua Zuo, and Chun-Li Zhang. 2021. "Revisiting Astrocyte to Neuron Conversion with Lineage Tracing in Vivo." *Cell*, September. https://doi.org/10.1016/j.cell.2021.09.005.

Xue, Yuanchao, Kunfu Ouyang, Jie Huang, Yu Zhou, Hong Ouyang, Hairi Li, Gang Wang, et al. 2013. "Direct Conversion of Fibroblasts to Neurons by Reprogramming PTB-Regulated microRNA Circuits." *Cell* 152 (1-2): 82–96.

Yoo, Sooyeon, David Cha, Dong Won Kim, Thanh V. Hoang, and Seth Blackshaw. 2019. "Tanycyte-Independent Control of Hypothalamic Leptin Signaling." *Frontiers in Neuroscience* 13 (March): 240.

Yoo, Sooyeon, Juhyun Kim, Pin Lyu, Thanh V. Hoang, Alex Ma, Vickie Trinh, Weina Dai, et al. 2021. "Control of Neurogenic Competence in Mammalian Hypothalamic Tanycytes." *Science Advances* 7 (22). https://doi.org/10.1126/sciadv.abg3777.

Zamboni, Margherita, Enric Llorens-Bobadilla, Jens Peter Magnusson, and Jonas Frisén. 2020. "A Widespread Neurogenic Potential of Neocortical Astrocytes Is Induced by Injury." *Cell Stem Cell* 27 (4): 605–17.e5.

Zhang, Lei, Jiu-Chao Yin, Hana Yeh, Ning-Xin Ma, Grace Lee, Xiangyun Amy Chen, Yanming Wang, et al. 2015. "Small Molecules Efficiently Reprogram Human Astroglial Cells into Functional Neurons." *Cell Stem Cell* 17 (6): 735–47.

Zhou, Haibo, Jinlin Su, Xinde Hu, Changyang Zhou, He Li, Zhaorong Chen, Qingquan Xiao, et al. 2020. "Glia-to-Neuron Conversion by CRISPR-CasRx Alleviates Symptoms of Neurological Disease in Mice." *Cell* 181 (3): 590–603.e16.
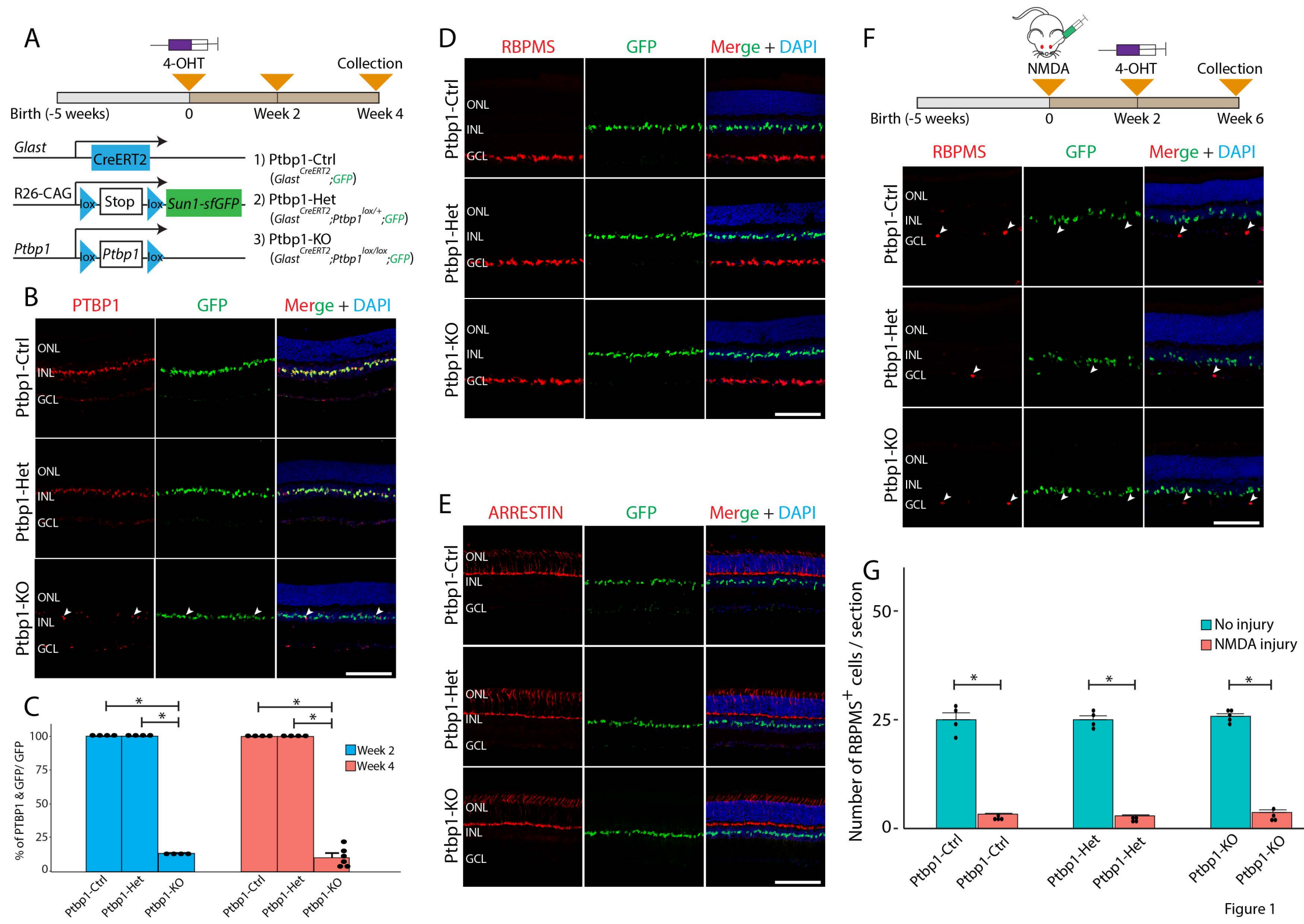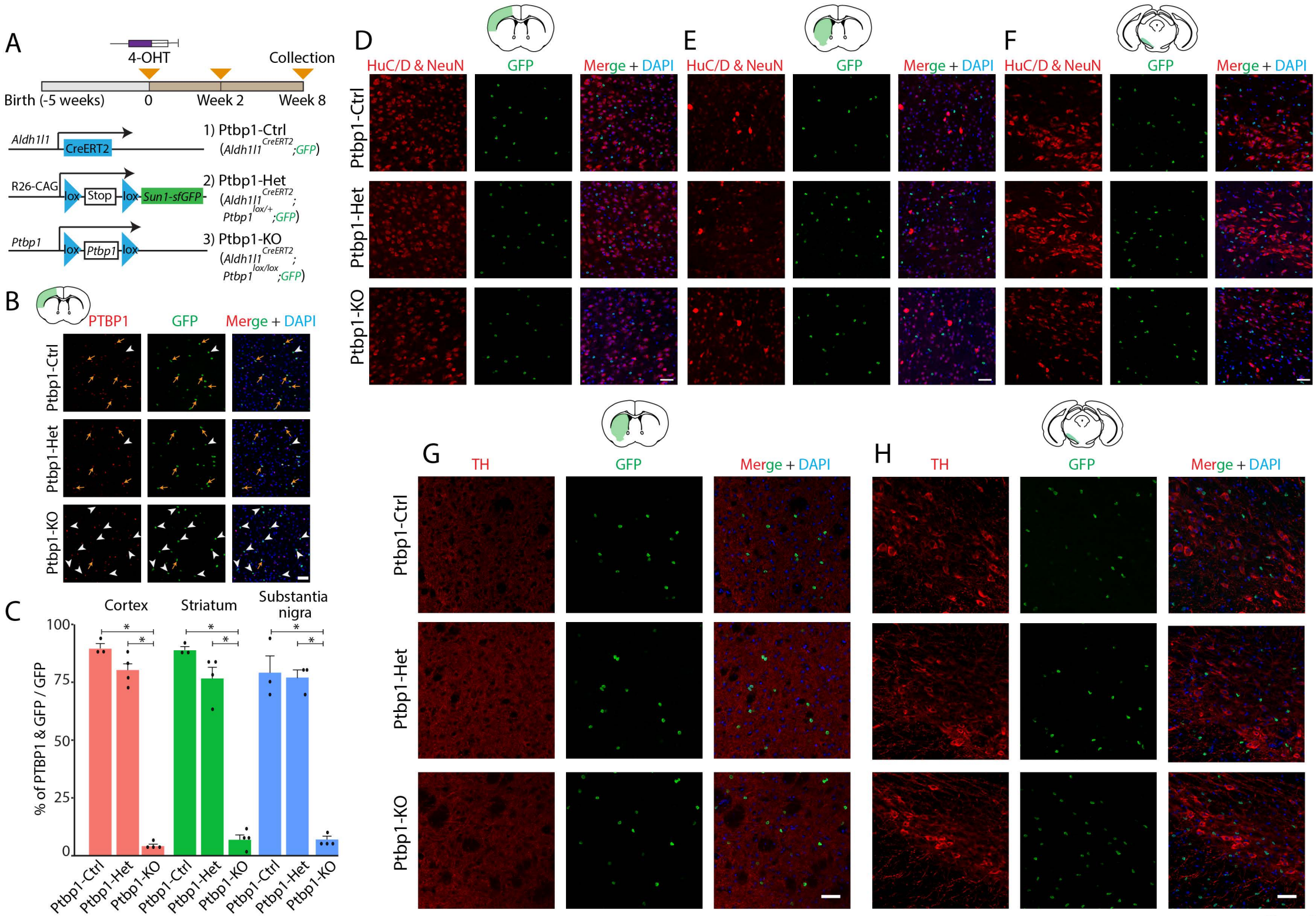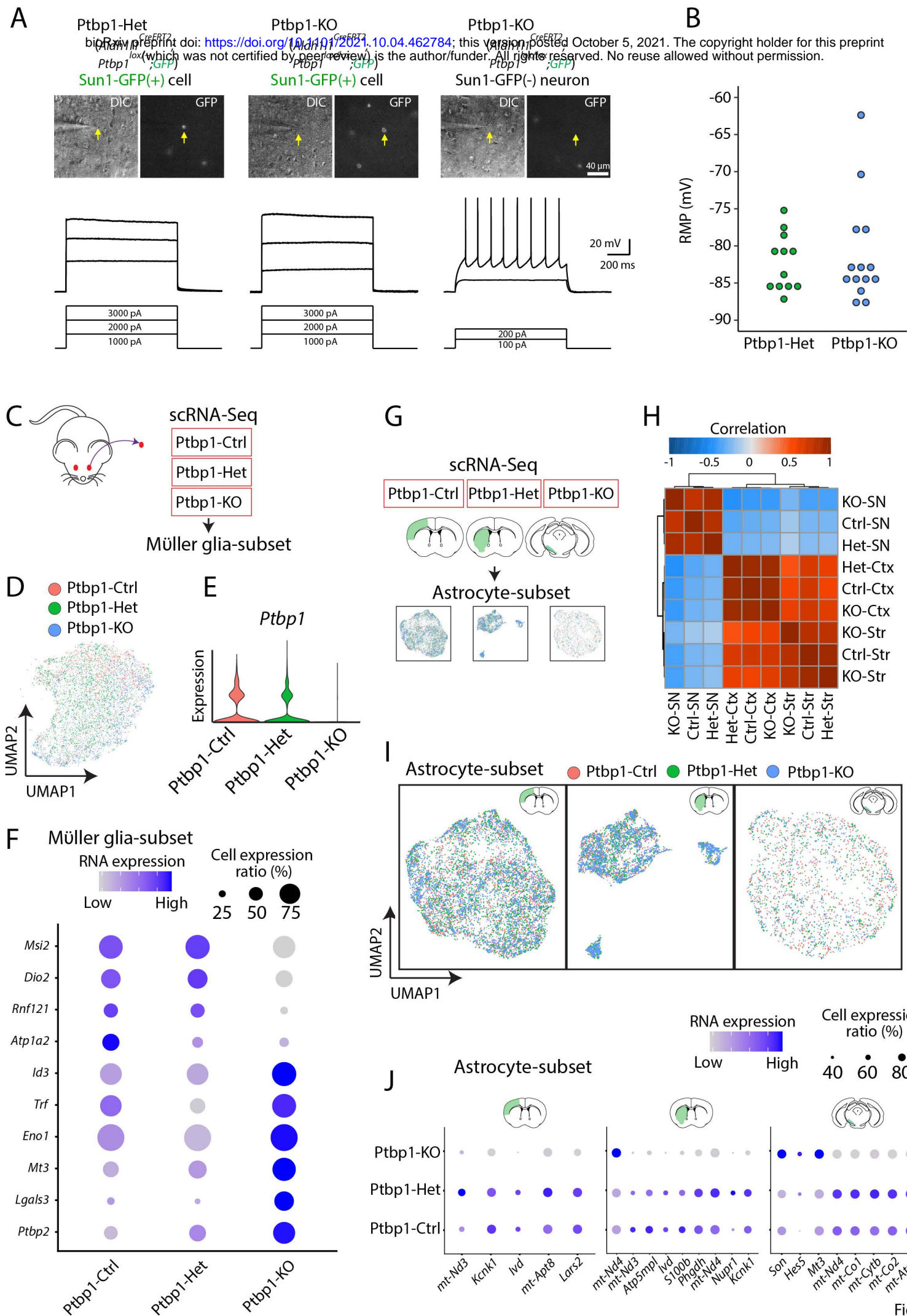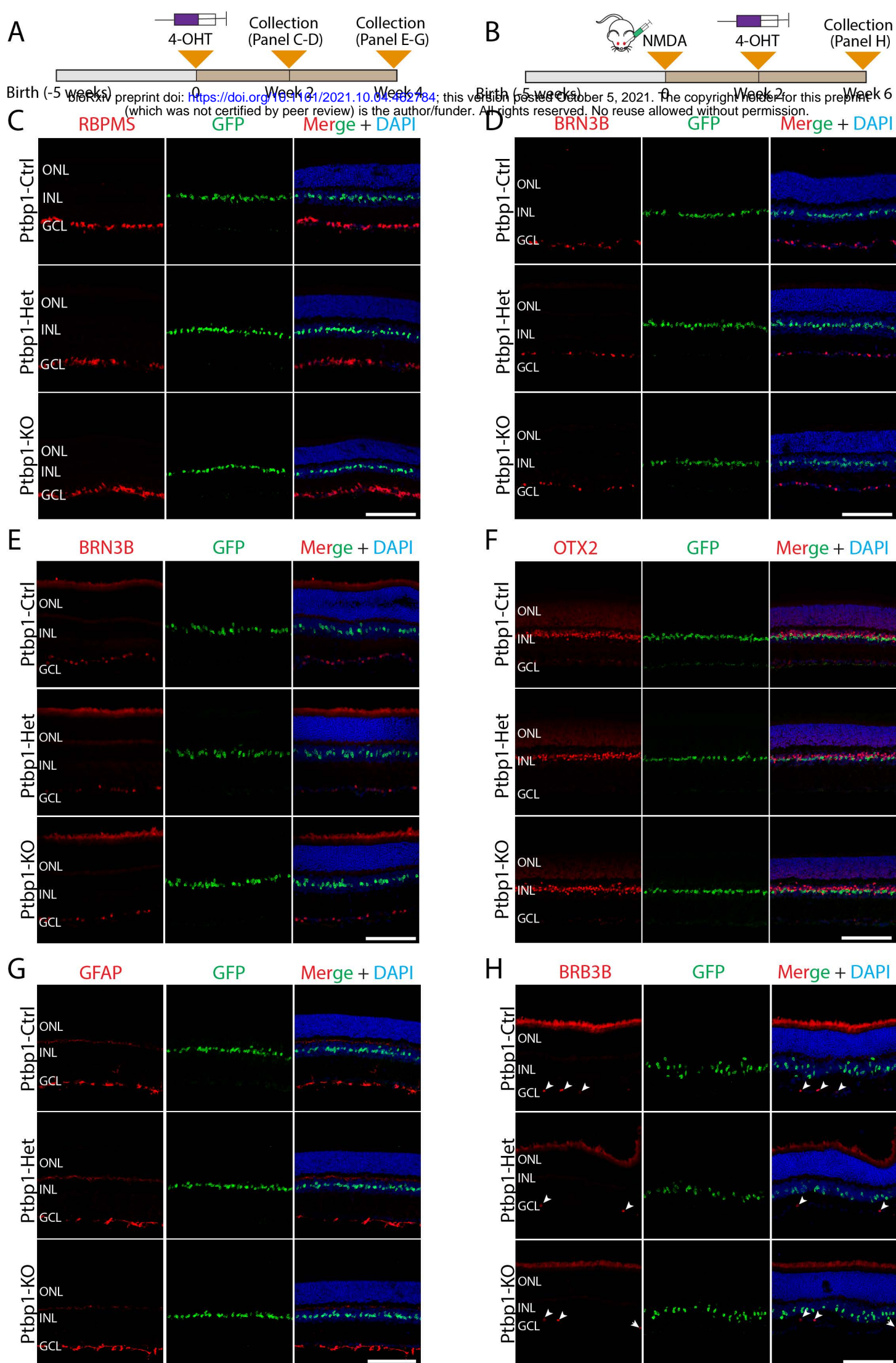
Figure 1

Figure 2

Figure 3

Figure S1

Figure S2

Figure S3

Figure S4

Figure S5